Concept Study of Optical Configurations for High-Frequency Telescope for LiteBIRD

T. Hasebe[22] · S. Kashima[34] · P. A. R. Ade[47] · Y. Akiba[19,49] · D. Alonso[41] · K. Arnold[16] · J. Aumont[20] · C. Baccigalupi[25] · D. Barron[48] · S. Basak[11,25] · S. Beckman[15] · J. Borrill[6,48] · F. Boulanger[20] · M. Bucher[3] · E. Calabrese[47] · Y. Chinone[15,29] · H.-M. Cho[28] · A. Cukierman[15] · D. W. Curtis[48] · T. de Haan[43] · M. Dobbs[42] · A. Dominjon[34] · T. Dotani[22] · L. Duband[18] · A. Ducout[29] · J. Dunkley[10,41] · J. M. Duval[18] · T. Elleflot[16] · H. K. Eriksen[24] · J. Errard[3] · J. Fischer[48] · T. Fujino[53] · T. Funaki[12] · U. Fuskeland[24] · K. Ganga[3] · N. Goeckner-Wald[15] · J. Grain[20] · N. W. Halverson[4,9,17] · T. Hamada[2,19] · M. Hasegawa[19,49] · K. Hattori[36] · M. Hattori[2] · L. Hayes[48] · M. Hazumi[19,22,29,49] · N. Hidehira[12] · C. A. Hill[15,43] · G. Hilton[38] · J. Hubmayr[38] · K. Ichiki[31] · T. Iida[29] · H. Imada[22] · M. Inoue[39] · Y. Inoue[19,21] · K. D. Irwin[13,28] · H. Ishino[12] · O. Jeong[15] · H. Kanai[53] · D. Kaneko[29] · N. Katayama[29] · T. Kawasaki[30] · S. A. Kernasovskiy[13] · R. Keskitalo[6,48] · A. Kibayashi[12] · Y. Kida[12] · K. Kimura[39] · T. Kisner[6,48] · K. Kohri[19] · E. Komatsu[33] · K. Komatsu[12] · C. L. Kuo[13,28] · N. A. Kurinsky[13,28] · A. Kusaka[14,43] · A. Lazarian[52] · A. T. Lee[15,43,44] · D. Li[28] · E. Linder[43,48] · B. Maffei[20] · A. Mangilli[20] · M. Maki[19] · T. Matsumura[29] · S. Matsuura[26] · D. Meilhan[48] · S. Mima[45] · Y. Minami[19] · K. Mitsuda[22] · L. Montier[5] · M. Nagai[34] · T. Nagasaki[19] · R. Nagata[19] · M. Nakajima[39] · S. Nakamura[53] · T. Namikawa[13] · M. Naruse[46] · H. Nishino[19] · T. Nitta[51] · T. Noguchi[34] · H. Ogawa[39] · S. Oguri[45] · N. Okada[23] · A. Okamoto[23] · T. Okamura[19] · C. Otani[45] · G. Patanchon[3] · G. Pisano[47] · G. Rebeiz[16] · M. Remazeilles[50] · P. L. Richards[15] · S. Sakai[22] · Y. Sakurai[29] · Y. Sato[23] · N. Sato[19] · M. Sawada[1] · Y. Segawa[19,49] · Y. Sekimoto[8,22,49] · U. Seljak[15] · B. D. Sherwin[7,27,43] · T. Shimizu[8] · K. Shinozaki[23] · R. Stompor[3] · H. Sugai[29] · H. Sugita[23] · A. Suzuki[15,44] · J. Suzuki[19] · O. Tajima[19,49] · S. Takada[35] · R. Takaku[53] · S. Takakura[19,40] · S. Takatori[19,49] · D. Tanabe[19,49] · E. Taylor[48] · K. L. Thompson[13,28] · B. Thorne[29,41] · T. Tomaru[19] · T. Tomida[22] · N. Tomita[1] · M. Tristram[32] · C. Tucker[16] · P. Turin[48] · M. Tsujimoto[22] · S. Uozumi[12] · S. Utsunomiya[29] · Y. Uzawa[37] · F. Vansyngel[20] · I. K. Wehus[24] · B. Westbrook[15] · M. Willer[48] · N. Whitehorn[15] · Y. Yamada[12] · R. Yamamoto[22] · N. Yamasaki[22] · T. Yamashita[53] · M. Yoshida[19]

✉ T. Hasebe
hasebe@astro.isas.jaxa.jp

[1] Aoyama Gakuin University, Sagamihara, Kanagawa 252-5258, Japan

Abstract The high-frequency telescope for LiteBIRD is designed with refractive and reflective optics. In order to improve sensitivity, this paper suggests the new optical configurations of the HFT which have approximately 7 times larger focal planes than that of the original design. The sensitivities of both the designs are compared, and the requirement of anti-reflection (AR) coating on the lens for the refractive option is derived. We also present the simulation result of a sub-wavelength AR structure on both surfaces of silicon, which shows a band-averaged reflection of 1.1–3.2% at 101–448 GHz.

Keywords Cosmic microwave background radiation · Inflation · Satellite · Telescope

[2] Astronomical Institute, Graduate School of Science, Tohoku University, Sendai 980-8578, Japan

[3] AstroParticule et Cosmologie (APC), Univ Paris Diderot, CNRS/IN2P3, CEA/Irfu, Obs de Paris, Sorbonne Paris Cité, France

[4] Center for Astrophysics and Space Astronomy, University of Colorado, Boulder, CO 80309, USA

[5] CNRS, IRAP, 31028 Toulouse Cedex 4, France

[6] Computational Cosmology Center, Lawrence Berkeley National Laboratory, Berkeley, CA 94720, USA

[7] DAMTP, University of Cambridge, Cambridge CB3 0WA, UK

[8] Department of Astronomy, The University of Tokyo, Tokyo 113-0033, Japan

[9] Department of Astrophysical and Planetary Sciences, University of Colorado, Boulder, CO 80309, USA

[10] Department of Astrophysical Sciences, Princeton University, Princeton, NJ 08544, USA

[11] School of Physics, Indian Institute of Science Education and Research Thiruvananthapuram, Maruthamala PO, Vithura, Thiruvananthapuram 695551, Kerala, India

[12] Department of Physics, Okayama University, Okayama 700-8530, Japan

[13] Department of Physics, Stanford University, Stanford, CA 94305-4060, USA

[14] Department of Physics, The University of Tokyo, Tokyo 113-0033, Japan

[15] Department of Physics, University of California, Berkeley, CA 94720, USA

[16] Department of Physics, University of California, San Diego, CA 92093-0424, USA

[17] Department of Physics, University of Colorado, Boulder, CO 80309, USA

[18] CEA, INAC-SBT, University of Grenoble Alpes, 38000 Grenoble, France

[19] High Energy Accelerator Research Organization (KEK), Tsukuba, Ibaraki 305-0801, Japan

[20] Institut d'Astrophysique Spatiale (IAS), CNRS, UMR 8617, Université Paris-Sud 11, Bâtiment 121, 91405 Orsay, France

[21] Institute of Physics, Academia Sinica, 128, Sec. 2, Academia Road, Nankang, Taiwan

[22] Institute of Space and Astronautical Science (ISAS), Japan Aerospace Exploration Agency (JAXA), Sagamihara, Kanagawa 252-0222, Japan

[23] Research and Development Directorate, Japan Aerospace Exploration Agency (JAXA), Tsukuba, Ibaraki 305-8505, Japan

[24] Institute of Theoretical Astrophysics, University of Oslo, 0315 Oslo, Norway

[25] International School for Advanced Studies (SISSA), Via Bonomea 265, 34136 Trieste, Italy

1 Introduction

LiteBIRD is a satellite mission to be launched by JAXA in the middle of the 2020s for verifying the inflation at the beginning of the universe via the B-mode polarization of the cosmic microwave background (CMB) [1,2]. The precise measurement of the B-mode signal requires the removal of contaminating polarized emissions, which mainly come from synchrotron and thermal dust. In order to separate these fore-

[26] Kansei Gakuin University, Nishinomiya, Hyogo 662-8501, Japan

[27] Kavli Institute for Cosmology Cambridge, Cambridge CB3 OHA, UK

[28] Kavli Institute for Particle Astrophysics and Cosmology (KIPAC), SLAC National Accelerator Laboratory, Menlo Park, CA 94025, USA

[29] Kavli Institute for the Physics and Mathematics of the Universe (Kavli IPMU, WPI), UTIAS, The University of Tokyo, Kashiwa, Chiba 277-8583, Japan

[30] Kitazato University, Sagamihara, Kanagawa 252-0373, Japan

[31] Kobayashi-Maskawa Institute for the Origin of Particle and the Universe, Nagoya University, Nagoya, Aichi 464-8602, Japan

[32] Laboratoire de l'Accélérateur Linéaire (LAL), Univ. Paris-Sud, CNRS/IN2P3, Université Paris-Saclay, Orsay, France

[33] Max-Planck-Institut for Astrophysics, 85741 Garching, Germany

[34] National Astronomical Observatory of Japan (NAOJ), Mitaka, Tokyo 181-8588, Japan

[35] National Institute for Fusion Science (NIFS), Toki, Gifu 509-5202, Japan

[36] National Institute of Advanced Industrial Science and Technology (AIST), Tsukuba, Ibaraki 305-8563, Japan

[37] National Institute of Information and Communications Technology (NICT), Kobe, Hyogo 651-2492, Japan

[38] National Institute of Standards and Technology (NIST), Boulder, CO 80305, USA

[39] Osaka Prefecture University, Sakai, Osaka 599-8531, Japan

[40] Osaka University, Toyonaka, Osaka 560-0043, Japan

[41] Oxford Astrophysics, Oxford OX1 3RH, UK

[42] Physics Department, McGill University, Montreal, QC H3A 0G4, Canada

[43] Physics Division, Lawrence Berkeley National Laboratory, Berkeley, CA 94720, USA

[44] Radio Astronomy Laboratory, University of California, Berkeley, CA 94720, USA

[45] RIKEN, Wako, Saitama 351-0198, Japan

[46] Saitama University, Saitama, Saitama 338-8570, Japan

[47] School of Physics and Astronomy, Cardiff University, Cardiff CF10 3XQ, UK

[48] Space Sciences Laboratory, University of California, Berkeley, CA 94720, USA

[49] The Graduate University for Advanced Studies (SOKENDAI), Miura District, Kanagawa, Hayama 240-0115, Japan

[50] The University of Manchester, Manchester M13 9PL, UK

[51] Division of Physics, Faculty of Pure and Applied Sciences, University of Tsukuba, Ibaraki 305-8571, Japan

ground emissions, LiteBIRD observes in frequency bands of 34–448 GHz with a low-frequency telescope (LFT) and high-frequency telescope (HFT). The frequency coverages of the LFT and the HFT were originally 34–270 and 238–448 GHz, respectively [3]. The accuracy of the foreground subtraction depends on the sensitivity of the observation band [4], and it strongly correlates with the number of detectors arranged in the limited focal plane area. To obtain a sensitivity gain, the focal plane area needs to be expanded by enlarging the size of the HFT. Expanding the focal plane area gives another advantage that it increases the sensitivity over an even broader frequency range, from 100–448 GHz covering the CMB spectra over 100 GHz. To realize such a broadband frequency coverage, a broadband AR coating should be developed on the lens if we choose a refractive design as the original design. The reason is that the reflection at a lens surface (for example, silicon causes approximately 30% reflection) makes a loss of the observation efficiency. Another option is to adopt reflective optics in order to avoid the concern about reflection of lenses. A comparison of the sensitivities of the options depends on the performance of the lens reflection. Therefore, in order to achieve a trade-off between these designs, it is necessary to set the requirement of lens reflection and to find out the AR coating of lens that meets this requirement.

2 Original Design of HFT

The schematic diagram of the original design of HFT is shown in Fig. 1. The optical design of the HFT basically follows that of typical refractive telescopes for CMB observations [5–7]. The HFT consists of a continuous—rotating half wave plate (HWP) [8], two silicon lenses, and feedhorn-coupled focal plane detectors [9]. The diameters of the objective lens and field lens are 245 and 175 mm, respectively, and their central thicknesses are 15.7 and 13.6 mm, respectively. In order to suppress thermal emissions from the optical elements, all the components are cooled down to less than 5 K. The superconducting detectors at the focal plane are required to operate at 100 mK including the optical loading. A 2 K aperture stop suppresses thermal loading of the spillover at the entrance pupil. The optical components are covered by millimeter-wave absorbers, which are pasted on the inner wall of the optics tube.

3 Large-Broadband HFT Designs

3.1 Optical Design

Figure 2 shows the candidates of the large HFT with refractive optics and reflective optics. The optical parameters of the HFT designs are summarized in Table 1. The optical elements of the refractive design are similar to those of the original design [3]. The diameters of the objective lens and field lens are 324 and 402 mm, respectively, and the central thicknesses are 19.8 and 26.4 mm, respectively. The reflective option with the Cross-Dragonian optical design [10] consists of a 675 mm $\times$ 585 mm primary

[52] University of Wisconsin-Madison, Madison, WI 53706, USA

[53] Yokohama National University, Yokohama, Kanagawa 240-8501, Japan

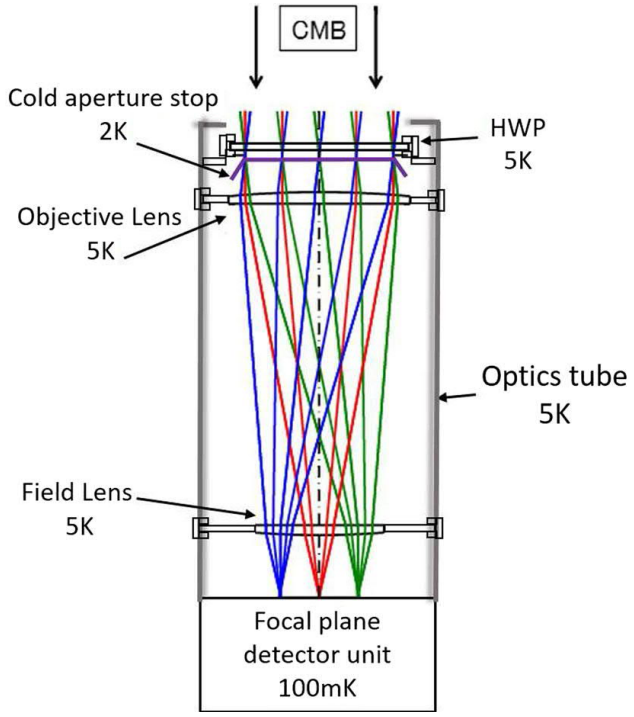

Fig. 1 Schematic view of the original design of HFT (Color figure online)

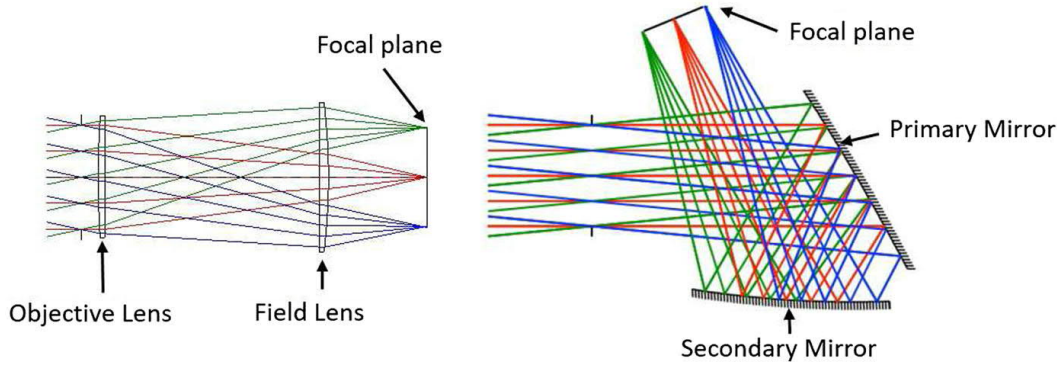

Fig. 2 (Left) Optical design of the large refractive HFT. (Right) Optical design of the reflective design (Color figure online)

Table 1 Optical parameters of the HFT designs. $F/\#$ represents the ratio of the effective focal length to the aperture diameter of an optical system

Model	Aperture diameter (mm)	$F/\#$	Field of view (deg^2)	Focal plane area (mm^2)
Original design	200	2.2	$\phi 13$	$\phi 102$
Large refractive design	300	2.2	$\phi 24$	$\phi 280$
Reflective design	300	3.5	20×10	370×184

mirror and a 656 mm $\times$ 600 mm secondary mirror. The optical parameters of each design are summarized in Table 2. The focal plane areas of the original, large refractive, and reflective designs are 81.7, 616, and 681 cm^2, respectively. Figure 3 shows the

Table 2 Parameters for sensitivity calculation

Parameter	Refractive	Reflective
F/#	2.2	3.5
Thickness of HWP	27 mm	27 mm
Refractive index of HWP	3.24	3.24
Loss tangent of HWP	5.0×10^{-5}	5.0×10^{-5}
Reflection of HWP	0.02	0.02
Resistivity of mirror		$1.39 \times 10^{-8}\Omega$
Surface roughness of mirror		2.0 μm
Thickness of lens	23 mm	
Refractive index of lens	3.42	
Loss tangent of lens	5.0×10^{-5}	

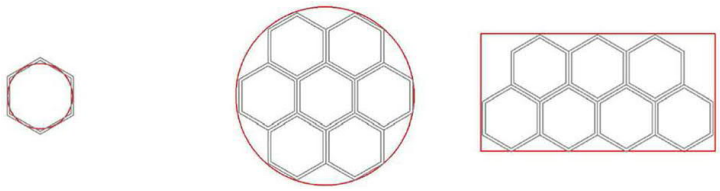

Fig. 3 Focal plane areas of the original (Left), the large refractive (Center), and the reflective (Right) designs and their wafer arrangements. The circular and rectangle geometries of the focal planes depend on the geometrical acceptances of the lenses and mirrors, respectively (Color figure online)

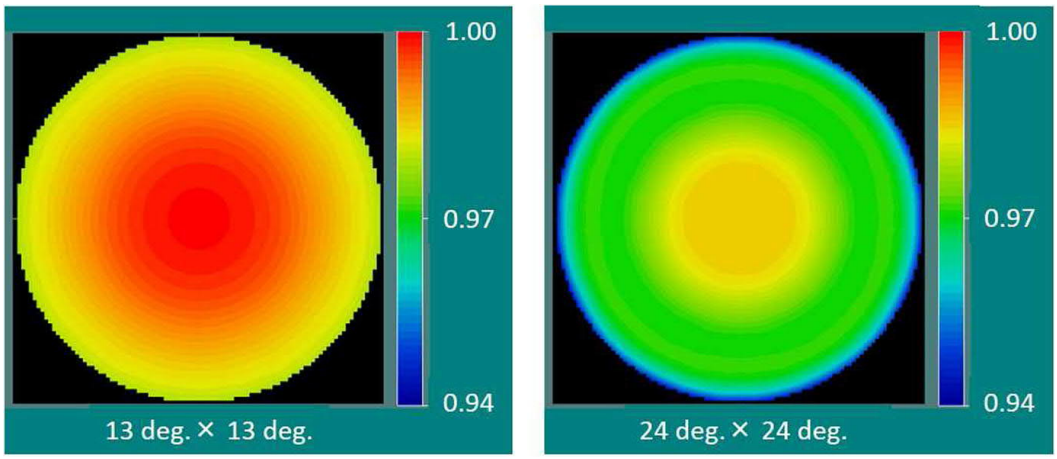

Fig. 4 Strehl ratios of the original (Left) and the large refractive designs (Right) at 450 GHz (Color figure online)

focal plane area of each design and the wafer arrangements on the assumption that the circumdiameter of the wafer is 100 mm. The Strehl ratios (the ratio of peak diffraction intensities of an aberrated wavefront to an ideal one) of the original and large refractive designs were evaluated as shown in Fig. 4, and they were found to be more than 0.98 and 0.94, respectively.

Table 3 Pixel size and the number of pixels per wafer in each band of the refractive option

Center frequency (GHz)	Band width ($\Delta\nu/\nu$)	Limited by the focal plane area		Limited by the number of detectors	
		Pixel size	Number of pixels	Pixel size	Number of pixels
119	0.30	7.5	91	12.4	37
166	0.30	6.2	127	9.4	61
235	0.30	4.5	217	6.2	127
280	0.30	3.9	271	6.2	127
337	0.30	3.4	331	5.2	169
402	0.23	3.0	397	4.5	217
Total			1476		738

3.2 Sensitivity Estimation

We assume that the frequency coverage of the broadband HFT is 101–448 GHz, and it is divided into 6 observation bands. The center frequencies and bandwidths of these bands are given in Table 3. To compare the available sensitivity for the broadband refractive and reflective options, the optimized pixel sizes of the detectors [11] in each band is evaluated for both cases under the assumption that the circular pixels are close-packed in a hexagonal area having a circumdiameter of 94 mm with a spacing of 1.0 mm between the edges of each pixel, and with a single-band feedhorn coupled to the detector. We note that, with a more practical arrangement, a multi-chroic lens is applicable to the bands of 119, 166, and 235 GHz, as is the case with the detectors for the LFT [12]. In this calculation, the detector noise consists of optical power loading, thermal carrier noise of the bolometer, and readout noise. The optical noise is calculated on the assumption that the CMB passes through a sapphire HWP and a couple of mirrors or silicon lenses, and is absorbed by a detector, which has a detection efficiency of 70% (The coupling between the antenna and the transmission line, the loss of the microstrip line, and the efficiency of the band pass filter are considered). The temperatures of the HWP, the mirrors, and the lenses are 5 K. The scattering of the mirrors and the reflections of the HWP and the lenses are terminated by the 5K absorbers. The spillover at the aperture stop is terminated at 2 K. The spillover efficiency at the aperture η_{apt} is given by $\eta_{\mathrm{apt}} = 1 - \exp(-\frac{\pi^2}{2}(\frac{D}{R_w F\lambda})^2)$ [13], where D is the pixel diameter, R_w is the ratio of D to the beam waist size, and λ is the wavelength. Here, we assume that $R_w = 3.1$ [14]. The equation of η_{apt} allows us to calculate the noise equivalent power (NEP) comes from the optical loading $\mathrm{NEP}_{\mathrm{opt}}$ as a function of the pixel diameter. The NEP originating from the thermal carrier noise of the bolometer $\mathrm{NEP}_{\mathrm{g}}$ is estimated as $\mathrm{NEP}_{\mathrm{g}} = 7.31 \times 10^{-12}\sqrt{P_{\mathrm{opt}}}$ [13], where P_{opt} is the optical power loading. We assume that the NEP of the readout component $\mathrm{NEP}_{\mathrm{read}}$ is 4.0 aW/$\sqrt{\mathrm{Hz}}$ in all the bands [15]. The total NEP of the single detector $\mathrm{NEP}_{\mathrm{tot}}$ is expressed as $\mathrm{NEP}_{\mathrm{tot}} = \sqrt{\mathrm{NEP}_{\mathrm{opt}}^2 + \mathrm{NEP}_{\mathrm{g}}^2 + \mathrm{NEP}_{\mathrm{read}}^2}$. The optimized pixel size is determined by the minimum value of the noise equivalent temperature (NET) on the

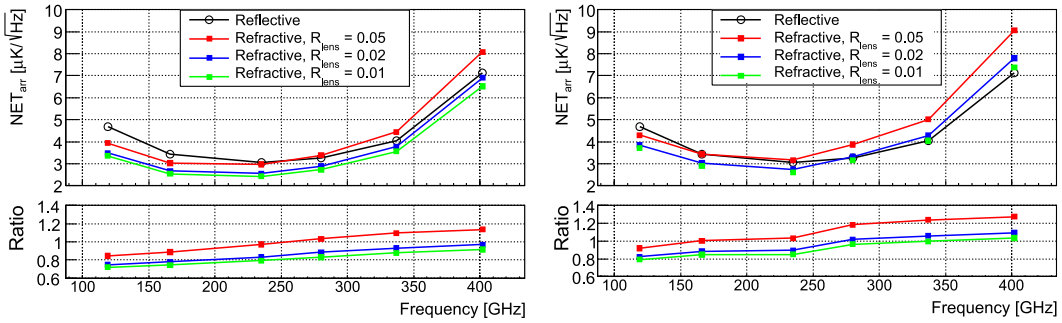

Fig. 5 (Left) Achievable sensitivities limited by the focal plane area. (Right) Sensitivities limited by the same number of detectors as the reflective option in each band. The bottom panels in both figures show the NET ratio of the refractive of corresponding colors to the reflective. The data points in both upper panels represent the $\mathrm{NET_{arr}}$ per single wafer (Color figure online)

CMB ($\mathrm{NET_{cmb}}$), which is given by $\mathrm{NET_{cmb}} = \frac{\mathrm{NEP_{tot}}}{\sqrt{2}(\mathrm{d}P/\mathrm{d}T_{\mathrm{cmb}})}$ [16]. The NET of each band $\mathrm{NET_{arr}}$ is defined as $\mathrm{NET_{arr}} = \mathrm{NET_{cmb}}/\sqrt{N_{\mathrm{det}}}$, where N_{det} is the number of detectors on a single hexagonal wafer, and it is twice as many as the number of pixels, because a single pixel has 2 polarimeters.

The achievable sensitivity of the broadband refractive and reflective designs are shown in the left part of Fig. 5. They are evaluated in such a way that each band takes the best sensitivity by choosing the optimized pixel diameter. If there are no constraints on the number of detectors and it is limited only by the focal plane area as shown in Fig. 3, the refractive option shows better sensitivity in all the bands compared to that of the reflective option, when the reflection of lenses (R_{lens}) are suppressed to less than 2%. However, the total number of detectors is an important evaluation criteria, since a higher number of detectors necessitates a higher number of readout systems and greater cooling power. As shown in the right part of Fig. 5, when N_{det} is limited to that for the reflective option, the $\mathrm{NET_{arr}}$ of the refractive option is 10% higher than that of the reflective option at the highest frequency band, when $R_{\mathrm{lens}} = 0.02$. The $\mathrm{NET_{arr}}$ at the lowest frequency band contrastively shows a 20% advantage. Therefore, the reasonable requirement for lens reflection should be $R_{\mathrm{lens}} < 0.02$. The pixel size and the number of pixels per wafer for both situations of the refractive option are given in Table 3.

4 Anti-reflection Coating of Silicon Lens

From the above discussion, it is seen that the AR coating of the silicon lens for the broadband refractive HFT requires less than 2% reflection. To achieve uniform AR performance in the broadband range, the Chebyshev transformer [18] is used for the AR coating of the lens. The AR performance of multi-layer dielectric thin films is simulated by using ANSYS HFSS [17]. At least 4 layers of coatings are necessary on both surfaces to meet the requirements of AR coating for the broadband HFT. The reflective index n_i and the thickness t_i of the i-th layer are designed as listed in Table 4. Applying a sub-wavelength structure (SWS) to realize similar performance as that of multi-layer AR coating is a powerful method in cryogenics applications, since it is

Table 4 Parameters of 4-layer thin-film AR coating

Layer	Vacuum	1st	2nd	3rd	4th	Substrate
n_i	1.00	1.24	1.60	2.13	2.74	3.42
d_i (mm)		219	171	128	100	

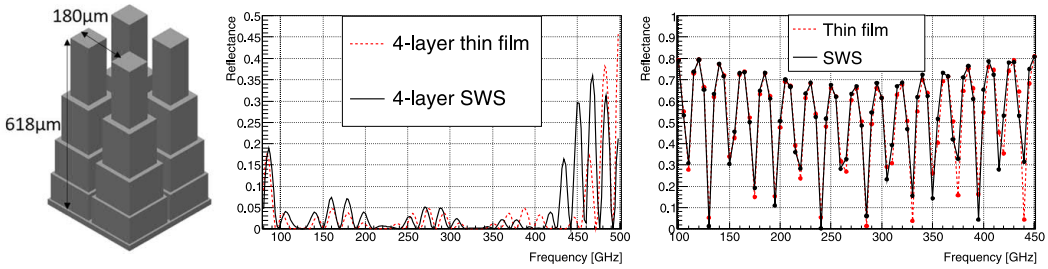

Fig. 6 (Left) 4-layer discrete SWS. (Center) Reflectances of the SWS and dielectric thin-film on both surfaces of silicon. (Right) Comparison of the frequency dependency of the reflectance between the SWS and dielectric thin-film of the first layer (Color figure online)

Table 5 Expected band-averaged reflection of the thin-film and SWS on both surfaces of silicon

Center frequency (GHz)	119	166	235	280	337	402
Reflection of thin-film (%)	0.7	2.0	0.8	1.6	1.2	1.4
Reflection of SWS (%)	1.5	3.2	1.1	1.8	1.1	2.8

possible to realize a SWS made of the same material as a lens. Therefore, there are no differences in thermal expansion between the material of the lens and AR layers. The left part of Fig. 6 shows the model of the discrete 4-layer SWS. The pitch of the pillars is designed to be 180 mm so that the 0th order diffraction appears at 500 GHz. Each layer has the same thickness as that of the thin-film design, and the filling rates of the structures are designed such that their effective refractive indices are consistent to that of the thin-film [19]. The reflective indices of the SWS and dielectric thin-film have different frequency dependencies; therefore, the filling rate of each layer of the SWS is adjusted in such a way that the refractive indices of the corresponding layers for both cases match at the center frequency of 275 GHz. The expected performance of the 4-layer SWS simulated by the HFSS is shown in the center part of Fig. 6. There is a mismatch in the reflectance above 350 GHz, since each layer shows the inconsistency of the reflectance between the thin-film and SWS at high frequency as shown in the right part of Fig. 6. The possible reason of it is the diffraction effect originating from the periodic structure of the SWS. The band-averaged reflectances of the thin-film and SWS are summarized in Table 5. The thin-film achieves less than 2% of reflection in all bands; however, the SWS does not satisfy this requirement at 166 and 402 GHz. Therefore, further optimization of the structure is needed.

The 2-layer silicon SWS with a dicing saw [20,21] and etching process [22] have already been performed. In the case of the multi-layer SWS as presented in this paper, etching process can be one of the solution, due to its high aspect ratio and precise structure comes from high-frequency coverage beyond 400 GHz. A silicon structure

which has aspect ratio more than 1:50 fabricated by deep reactive-ion etching has been reported by [23,24].

5 Conclusion

The conceptual designs of the HFT, including large and broadband refractive and reflective designs, were discussed. The performance of lens reflection is a key parameter for evaluating the trade-off between the refractive and the reflective options. The refractive design requires less than 2% lens reflection to achieve an equivalent sensitivity to that of the reflective design with the same number of detectors. The expected performance of the 4-layer SWS type AR coating is demonstrated, and it shows a band-averaged reflection of 1.1–3.2% at 100–450 GHz.

Acknowledgements This work was supported by JSPS/MEXT KAKENHI Grant Numbers 17H01115 and 15H05891.

References

1. M. Hazumi et al., *Proceedings of SPIE* **8442** (2012). https://doi.org/10.1117/12.926743
2. H. Ishino et al., *Proceedings of SPIE* **9904** (2016). https://doi.org/10.1117/12.2231995
3. H. Sugai et al., *Proceedings of SPIE* **9904** (2016). https://doi.org/10.1117/12.2232008
4. N. Katayama, E. Komatsu, Astrophys. J. **737**, 78 (2011). https://doi.org/10.1088/0004-637X/737/2/78
5. A.S. Rahlin et al., *Proceedings of SPIE* **9153** (2014). https://doi.org/10.1117/12.2055683
6. P.A.R. Ade et al., Astron. J. **806**, 206 (2015). https://doi.org/10.1088/0004-637X/806/2/206
7. J. Bock et al., arXiv:0805.4207
8. T. Matsumura et al., IEEE Trans. Appl. Supercond. **26**, 3 (2016). https://doi.org/10.1109/TASC.2016.2533584
9. J. Hubmayr et al., J. Low Temp. Phys. **167**, 904 (2012). https://doi.org/10.1007/s10909-011-0420-7
10. S. Kashima et al., (in preparation)
11. S. Padin, Appl. Opt. **49**, 3 (2010). https://doi.org/10.1364/AO.49.000479
12. B. Westbrook et al., J. Low Temp. Phys. **184**, 74 (2016). https://doi.org/10.1007/s10909-016-1508-x
13. A. Suzuki, *Ph.D. dissertation* (University of California, Berkeley, 2013)
14. A. Gonzalex, Yoshinori Uzawa, IEEE Trans. Antennas Propag. **60**, 7 (2012). https://doi.org/10.1109/TAP.2012.2196960
15. T. Matsumura et al., J. Low Temp. Phys. **184**, 824 (2016). https://doi.org/10.1007/s10909-016-1542-8
16. K. Arnold, *Ph.D. dissertation* (University of California, Berkeley, 2010)
17. http://www.ansys.com/products/electronics/ansys-hfss/
18. D.M. Pozar, *Microwave Engineering* (John Wiley & Sons Inc, 1998)
19. E.B. Grann, M.G. Moharam, D.A. Pommet, J. Opt. Soc. Am. A **11**, 10 (1994). https://doi.org/10.1364/JOSAA.11.002695
20. R. Datta et al., Appl. Opt. **52**, 36 (2013). https://doi.org/10.1364/AO.52.008747
21. T. Nitta et al., IEEE Trans. Terahertz Sci. Technol. **7**, 3 (2017). https://doi.org/10.1109/TTHZ.2017.2692045
22. P.A. Gallardo et al., Appl. Opt. **56**, 10 (2017). https://doi.org/10.1364/AO.56.002796
23. A. Kok et al., *IEEE NSS/MIC Conference Record* (2009). https://doi.org/10.1109/NSSMIC.2009.5402256
24. Y. Tang et al., *IEEE MEMS* (2017). https://doi.org/10.1109/MEMSYS.2017.7863504